CHEMISTRY OF MATERIALS

ARTICLE

pubs.acs.org/cm

Controlled Fabrication of Colloidal Semiconductor−Metal Hybrid Heterostructures: Site Selective Metal Photo Deposition

Mussie G. Alemseghed, T. Purnima A. Ruberu, and Javier Vela*

Department of Chemistry, Iowa State University, and U.S. Department of Energy Ames Laboratory, Ames, Iowa 50011, United States

Supporting Information

ABSTRACT: Reliable synthesis of semiconductor−metal heterostructures would increase their availability for fundamental studies and applications in catalytic, magnetic, and opto-electronic devices. Here, we demonstrate there are three main pathways for the formation of Pt and Pd nanoparticles on CdS and $CdS_{0.4}Se_{0.6}$ nanorods. A thermal pathway and photochemical pathway occur when the metal precursor is heated or irradiated directly in the presence of an electron donor, leading to homogeneous nucleation and formation of freestanding metal nanoparticles. A separate photochemical pathway occurs in the presence of semiconductor nanorods, leading to exciton formation and quenching by electron trapping at surface defect sites. The localized electrons act as seeding points, leading to heterogeneous nucleation and formation of surface-bound metal nanoparticles. Careful selection of synthetic conditions allows deposition of Pt and Pd particles on CdS and $CdS_{0.4}Se_{0.6}$ nanorods with a high degree of selectivity (90−95% surface-bound obtained photochemically) over the formation of freestanding metal particles (70−94% unattached under thermal conditions). In addition, metal photo deposition occurs on specific segments of $CdS_{0.4}Se_{0.6}$ nanorods with compositional anisotropy by taking advantage of the band gap differential between different nanodomains. Irradiation at short wavelengths favors formation of Pd nanoparticles on the large band gap CdS-rich region of the nanorods (57% and 55% at 350 and 420 nm, respectively), while irradiation at longer wavelengths favors the formation of Pd nanoparticles on the small band gap CdSe-rich region of the nanorods (83% at 575 nm). The ability to tune the spatial composition of these and similar heterostructures will impact the ability to engineer and direct energy flows at the nanoscale.

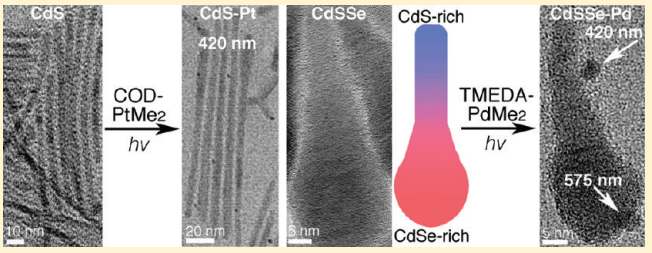

KEYWORDS: semiconductor, metal, heterostructure, hybrid, photo deposition, site selectivity

INTRODUCTION

Semiconductor−metal hybrid heterostructures are promising building blocks for applications in catalytic, magnetic, and opto-electronic devices.[1−7] The semiconductor's tunable band gap (300−4000 nm 4.1−0.3 eV),[8,9] broad and intense absorption ($\varepsilon \approx 10^5$−10^6 L mol^{-1} cm^{-1}),[10] and long-lived exciton (up to 40 ns for CdSe, 1.8 μs for PbS)[11,12] provide unmatched light absorption and emission capabilities. Large aspect ratio semiconductors such as nanorods are of particular interest because of their ability to generate multiple excitons.[13,14] The metal can serve as an additional chromophore, fluorescence enhancer, paramagnet, or charge-collecting material where carriers localize after exciton quenching. For example, semiconductor−metal hybrid heterostructures have been shown to convert solar energy into potential and chemical energy. They become redox-active upon illumination and remain redox-active after being stored in the dark for several hours.[15] In addition, semiconductor and metal nanocrystals display a high degree of chemical-, photo-, and colloidal-stability (solubility) unmatched by other materials such as organic polymers and transition metal complexes. The ability to selectively build semiconductor−metal heterostructures with several morphologies and spatial relationships between their individual components could be used to engineer and direct energy flows at the nanoscale.[4]

Interest in the synthesis of colloidal semiconductor−metal hybrid nanostructures has grown exponentially in recent years.[1,2] Different research groups have used thermal and photochemical methods to synthesize CdS, CdSe, and core/shell CdSe/CdS nanorods tipped with Au,[16−20] Ag_2S,[19] Co,[21,22] Pt, PtM (M = Co, Ni),[23] PdO and Pd_4S[24] nanoparticles, ZnO nanorods-tipped with Ag nanoparticles,[25] a-TiO_2 nanorods tipped with Co nanoparticles,[26] and CdSe tetrapods tipped with Au nanoparticles.[18] Similarly, metal nanoparticle deposition along the whole length of semiconductor nanorods has been demonstrated for CdS−Au,[16,27] CdSe/CdS−Au,[19] CdSe−Pt,[28] CdS−PdO and CdS−Pd_4S,[24] CdS−Pt,[29] CdSe/CdS−Pt,[29] CdS−FePt,[30] and a-TiO_2−Co.[26] Other reports include CdSe nanowires decorated with Au, Pt, PtCo, and PtNi nanoparticles,[31] PbS nanocubes coated with Au nanoparticles,[32] and nanoporous CdS loaded with Pt nanoparticles.[33] Some of these reports build upon earlier work on the surface modification of microcrystalline semiconductors using platinum group metals as a way to generate hydrogen evolving photocatalysts, for example, CdS−Pt doped wth Zn and Ag sulfides,[34,35] and powders made of MS/CdS/M(M = Pt, Ir),[36]

Received: May 27, 2011
Revised: June 27, 2011
Published: July 13, 2011

CdS_xSe_{1-x}−Pt,[37] CdS/Pt/Na_2S,[38] CdS−Pt and TiO_2−Pt,[39] and CdS/TiO_2.[40]

Perhaps the most important aspect from a synthetic perspective is to prepare semiconductor−metal and other semiconductor-based hybrid heterostructures with "open" (noncore/shell)[41,42] configurations in a controlled and selective fashion. Reliable synthetic routes would increase the availability of these materials for fundamental study and systematic testing, allowing the establishment of structure−activity relationships and facilitating their eventual application. It is valuable to investigate selective syntheses of colloidal semiconductor−metal heterostructures that are highly reproducible and amenable to scaleup. In the case of CdS−Au heterostructures, photochemical deposition leads to growth of Au particles at the tips of CdS nanorods, whereas thermal deposition (in the dark) leads to growth of Au particles along the whole length of CdS nanorods.[1,43] Deposition throughout the semiconductor surface is more desirable for solar energy harvesting because it could lead to more efficient multiple exciton quenching via charge separation. The opposite trend is observed in CdS−Pt heterostructures, where photochemical deposition leads to growth of Pt particles along the whole length of CdS nanorods,[29] and thermal deposition at high temperature (200 °C) leads to growth of Pt particles at the CdS nanorod tips.[23] The exact deposition behavior varies depending on the particular metal and semiconductor surface under study. For CdS−PtM (M = Ni, Co), thermal deposition at low precursor concentrations results in PtM particles at the CdS nanorod tips (particularly for PtCo), whereas thermal deposition at high concentrations results in PtM particles along the whole length of the CdS nanorods.[23] For CdSe/CdS−Au and CdSe/CdS−Pt heterostructures, the position of the Au and Pt particles correlates with the position of CdSe core or "seed".[16,29] For CdSe/CdS−AuPd and CdSe/CdS−$AuFe_xO_y$ heterostructures, ultraviolet irradiation results in particles at the CdSe/CdS nanorod tips.[44] A majority of the documented photochemical deposition methods on nanostructures employ laser irradiation,[16,17,19,25] which invariably occurs over small sample areas or "spots", leading to low material yields and thus limiting its synthetic utility. Few researchers and virtually no synthetic chemists have direct and reliable access to expensive lasers.

In this paper, we use thermal and large throughput lamp photochemical methods to address the controllable and site selective deposition of metal nanoparticles on single-phase and heterostructured semiconductor nanorods. We use Pt and Pd deposition on regular CdS nanorods in addition to axially anisotropic $CdS_{1-x}Se_x$ nanorods as model systems. On the basis of the results of several deposition experiments under different temperature and illumination conditions, the formation of metal particles proceeds by at least three fundamental pathways. Two of these pathways, one thermal and one photochemical, are independent of the semiconductor surface and lead to the formation of freestanding metal particles. A third photochemical pathway is mediated by the semiconductor and leads to formation of surface-bound metal particles, which are preferred because many semiconductor−metal interactions such as charge- and energy-transfer are strongly distance dependent. Selection of experimental conditions allows synthesis of surface-bound particles with a high degree of selectivity over formation of freestanding (unattached) metal particles. We also demonstrate photo deposition of metal particles can be controllably directed toward specific segments or regions of a heterostructured semiconductor with compositional anisotropy by taking advantage of the inherent band gap and optical properties of its different segments or "nanodomains".

EXPERIMENTAL SECTION

Materials. Cadmium oxide (99.998%) and sulfur (99.999%) were purchased from Alfa Aesar. Octadecylphosphonic acid (ODPA) was purchased from PCI Synthesis. Selenium (99.999%), trioctylphosphine oxide (TOPO) (99%), and triethylamine (≥99.5%) were purchased from Sigma-Aldrich. Trioctylphosphine (TOP) (97%), dimethyl(1,5-cyclooctadiene)platinum(II) (CODPtMe_2, 99%) and cis-dimethyl(N,N,N′,N′-tetramethylenediamine)palladium(II) (TMEDAPdMe_2, 99%) were purchased from Strem. All chemicals were used as received unless specified otherwise. *Caution*: Appropriate personal protective equipment and engineering controls must be in place before the use of cadmium, a toxic heavy metal.

Photochemical Experiments. Photochemical experiments were conducted in a fan-cooled Rayonette photoreactor (Southern New England Ultraviolet Company, Branford, CT) equipped with an air-cooling fan and a carousel unit. Between 2 and 16 (max) 12 in. side-on "fluorescent" lamps (Luzchem, Ottawa, Ontario) were used for each experiment.

Synthesis of Colloidal CdS and CdSSe Nanorods. *CdS Nanorods.* CdS nanorods (154.1 ± 30.4 nm length, 5.6 ± 0.8 nm diameter) were prepared according to a reported literature procedure.[45] The CdS nanorods were found to have a wurtzite crystal structure.[46]

CdSSe Nanorods. Axially anisotropic $CdS_{0.4}Se_{0.6}$ nanorods having a "drumstick"-like morphology (59.3 ± 8.0 length, 17.8 ± 2.4 nm "head" diameter, 5.6 ± 0.8 nm "tail" diameter) were synthesized by a modified procedure recently reported by our group.[46] Briefly, CdO (105 mg, 0.81 mmol), TOPO (1.375 g, 3.56 mmol), and ODPA (535 mg, 0.94 mmol) were weighed onto a three-neck round-bottomed flask. The flask was fitted with a glass-coated magnetic stir bar, condenser, and stainless steel thermocouple. The apparatus was sealed and brought onto an Schlenk line. Using a heating mantle, the mixture was heated to 100 °C and evacuated under vacuum for 15 min, and then it was refilled with argon and heated to 320 °C to form a completely colorless solution. The solution was then allowed to cool to 120 °C and evacuated under vacuum for 15 min, and then refilled with argon and heated back to 320 °C. When the temperature reached 300 °C, TOP (1.20 mL, 2.7 mmol) was injected into the flask. When the temperature reached 320 °C, a solution containing an air-free mixture of 2.25 M TOPS (0.90 mL, 2 mmol) and 2.25 M TOPSe (0.10 mL, 0.2 mmol) was rapidly injected, causing a gradual color change. Upon injection, the temperature was allowed to equilibrate at 315 °C and kept constant for a total reaction time of 85 min. The reaction mixture was then removed from the heating mantle and allowed to cool to room temperature. After dilution with toluene (5 mL), the nanorods were isolated by the addition of a 1:1 v/v iso-propanol/nonanoic acid (24 mL) mixture, followed by centrifugation (5000 rpm for 10 min). The $CdS_{0.4}Se_{0.6}$ nanorods were found to have a wurtzite crystal structure.[46]

Synthesis of CdS−Pt and CdS−Pd Heterostructures. CdS nanorods were dissolved in toluene to give an optical density (OD) of 1.2 at 470 nm. A 2 mL volume of this solution was degassed, refilled with dry argon, and stored in the dark for 12 h in a resealable Schlenk tube. Under a dry atmosphere, CODPtMe_2 (28 mg, 0.08 mmol) for CdS−Pt or cis-dimethyl-(N,N,N′,N′-tetramethylene-diamine)palladium(II) (TMEDAPdMe_2) (28 mg, 0.1 mmol) for CdS-Pd was dissolved in anhydrous toluene (1 mL), mixed with triethylamine (0.5 mL, used as a terminal electron donor),[29] and added to the CdS nanorod solution via syringe. The deposition reaction was then carried out for 3 h by one of two routes: (1) *Thermally* in the dark, in an oil bath pre-equilibrated at 80 °C for CdS−Pt or in a room temperature (RT) water bath for CdS−Pd or (2)

photochemically, under illumination at room temperature (21−24 °C) in a fan-cooled Rayonet photoreactor containing a set of 16 side-on fluorescent lamps (350 or 420 nm, see below) (total intensities: 136 and 16.6 W/m^2, respectively). The nonvolatile products were purified by precipation with a 1:1 mixture of acetone and methanol (30 mL) and centrifugation (4200 rpm for 10 min). All products readily redisperse in toluene.

Synthesis of $CdS_{0.4}Se_{0.6}$−Pd Heterostructures. Axially anisotropic $CdS_{0.4}Se_{0.6}$ nanorods[46] were dissolved in toluene to give an optical density (OD) of 1.3 at 630 nm. A 2.0 mL volume of this solution was degassed, refilled with dry argon, and stored in the dark for 12 h in a resealable Schlenk tube. Under a dry atmosphere, (TMEDA)$PdMe_2$ (30 mg, 0.1 mmol) was dissolved in anhydrous toluene (1 mL), mixed with triethylamine (0.5 mL, used as terminal electron donor),[45] and added to the $CdS_{1-x}Se_x$ nanorod solution via syringe. The deposition reaction was then carried out for 1 or 3 h photochemically under illumination at room temperature (21−24 °C) in a fan-cooled Rayonet photoreactor containing a set of 16 side-on fluorescent lamps (350 nm, 420 or 575 nm, see below) (total intensities: 136, 16.6, and 47.2 W/m^2, respectively). The nonvolatile products were purified twice by precipation with methanol (30 mL) and centrifugation (5000 rpm for 10 min). All products could be readily redispersed in toluene.

Structural Characterization. *X-ray Diffraction.* Powder X-ray diffraction (XRD) data were measured using Cu Kα radiation on a Scintag XDS-2000 diffractometer equipped with a theta−theta goniometer, a sealed-tube solid-state generator, and an air-cooled Kevex Psi Peltier silicon detector. The XRD samples were prepared by spreading solid nanocrystal samples onto a background-less quartz sample holder.

Transmission Electron Microscopy. Transmission electron microscopy (TEM) was conducted using a FEI Technai G2 F20 field emission TEM and a scanning transmission electron microscope (STEM) operating at 200 kV. This instrument has a point-to-point resolution of less than 0.25 nm and a line-to-line resolution of less than 0.10 nm. TEM samples were prepared by placing 2−3 drops of dilute toluene solutions of the nanocrystals onto carbon-coated copper grids. The elemental axial distribution and composition of the nanorods were characterized by energy dispersive spectroscopy (EDS) line scans in STEM mode, as well as by energy-filtered (EF) imaging spectroscopy (EF-TEM) using a Gatan Tritium GIF system.

Size and Morphology Analysis. Particle dimensions were measured manually and/or with ImageJ. In all cases, measurements and statistics were obtained for at least 50−100 nanorods (CdS or $CdS_{0.4}Se_{0.6}$) and 50−300 metal particles (Pt, Pd). Uncertainties in all measurements are reported as the standard deviations.

Optical Characterization. Absorption spectra were measured in 0.1 or 1 cm quartz cuvettes with a photodiode array Agilent 8453 UV−vis spectrophotometer. The absorption of the solvent was recorded and subtracted from all spectra. The absorption coefficients (ε/L mol^{-1} cm^{-1}) of organometallic precursors were measured according to Lambert−Beer's Law by carefully preparing and recording the absorbance of different solutions in toluene.

RESULTS AND DISCUSSION

To date, most colloidal semiconductor−metal heterostructures have been fabricated by decomposing soluble organometallic precursors or salts in the presence of semiconductor nanorods. This is accomplished by simple heating in some cases, such as deposition of Au particles along the length of CdS nanorods.[1,16] Better control over metal deposition, particularly Pt, has been reported using laser spot irradiation leading to growth of Pt particles along the length of CdS nanorods.[23,29] Exploring the feasibility of synthesizing hybrid heterostructures without use of lasers, we observed deposition of Pt and Pd on colloidal

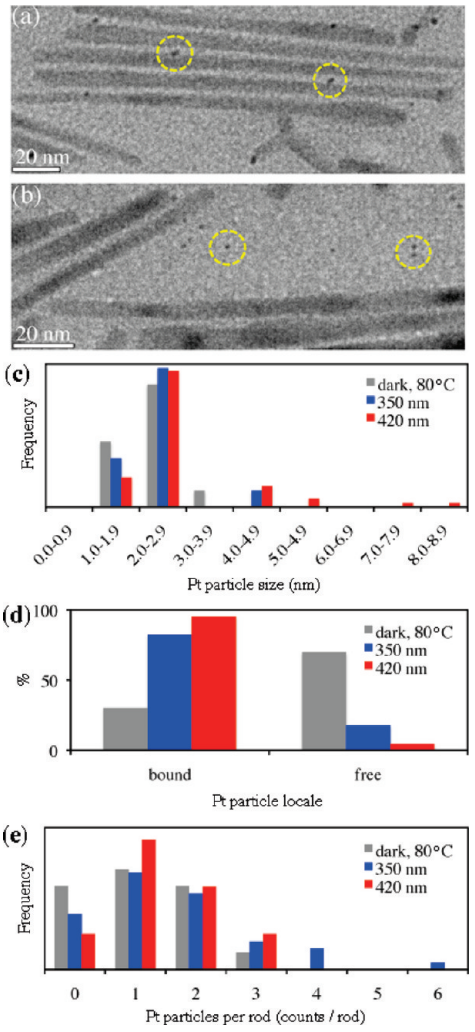

Figure 1. Sample TEM micrographs of CdS−Pt heterostructures prepared (a) photochemically (420 nm, RT), and (b) thermally (in the dark, 80 °C) (a few surface-bound and freestanding Pt particles are circled for comparison). Pt particle size (c), locale (d), and loading per rod (e) histograms for CdS-Pt heterostructures prepared thermally (80 °C in the dark, gray) and photochemically (350 nm, blue; 420 nm, red) (>50−100 CdS rods and >50−300 Pt particles measured in each case).

CdS and $CdS_{1-x}Se_x$ nanorods could be easily carried out with an inexpensive set of lamps. Lamps illuminate much larger areas at a time compared to lasers (whole samples in this study as well as other recent studies);[17,25,44,47] their use could lead to a larger synthetic throughput and wider general availability of semiconductor−metal hybrid heterostructures for fundamental studies and application. While metal deposition should be possible with any lamp whose energy sat below the band gap of the semiconductor (i.e., <520 nm or >2.4 eV for CdS nanorods), we find the precise mechanism and locale of metal deposition varies greatly depending on the specific irradiance profile of the lamp used.

Platinum Deposition on CdS Nanorods. We first attempted to deposit Pt on CdS nanorods termally at 80 °C in the complete absence of light. Thermal deposition in the dark results in the formation of small Pt particles with a diameter of 1.9 ± 0.6 nm as observed by transmission electron microscopy (TEM) (Figure 1). However, the great majority of the thermally deposited Pt particles

Table 1. Metal Deposition on Colloidal Semiconductor Nanorods[a]

no.	nanorods	M	precursor	conds.[a]	T (°C)	rxn. time (h)	np. diameter (nm)	% bound	% free	np./rod
1	CdS	Pt	$CODPtMe_2$	dark	80	3	1.9 ± 0.6	30	70	1.1 ± 0.9
2	CdS	Pt	$CODPtMe_2$	350 nm	24	3	2.6 ± 0.8	80	20	1.6 ± 1.3
3	CdS	Pt	$CODPtMe_2$	420 nm	24	3	3.1 ± 1.4	95	5	1.4 ± 0.9
4	None	Pt	$CODPtMe_2$	420 nm	24	3	2.9 ± 1.2	–	–	–
5	CdS	Pd	TMEDA-$PdMe_2$	420 nm	24	3	7.2 ± 1.7	90	10	5.6 ± 2.2
6	CdS	Pd	TMEDA-$PdMe_2$	dark	24	3	4.1 ± 0.7	6	94	2.1 ± 0.7
7	$CdS_{0.4}Se_{0.6}$	Pd	TMEDA-$PdMe_2$	350 nm	24	1	2.6 ± 0.8	37	63	1.5 ± 1.1
8	$CdS_{0.4}Se_{0.6}$	Pd	TMEDA-$PdMe_2$	420 nm	24	1	4.9 ± 2.2	48	52	2.1 ± 1.5
9	$CdS_{0.4}Se_{0.6}$	Pd	TMEDA-$PdMe_2$	575 nm	24	1	5.0 ± 1.5	90	10	1.3 ± 0.8
10	$CdS_{0.4}Se_{0.6}$	Pd	TMEDA-$PdMe_2$	575 nm	24	3	5.1 ± 1.4	92	8	8.0 ± 2.0

[a] All reactions were carried out using a 2 mL nanorod solution in toluene of $OD_{470\ nm}$ = 1.2 (CdS) or $OD_{630\ nm}$ = 1.3 ($CdS_{0.4}Se_{0.6}$), 28−30 mg metal precursor, 0.5 mL NEt_3 as electron donor, and 1 mL toluene. See Experimental Section.

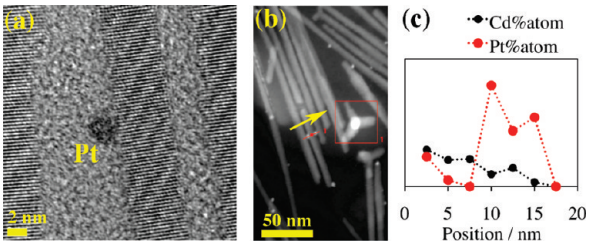

Figure 2. (a) High-resolution (HR) TEM micrograph of a surface-bound Pt particle produced via photochemical deposition on CdS nanorods (420 nm, 3 h). (b) EDX-Line scan and (c) corresponding composition profile of two Pt nanoparticles attached to opposing sides of a CdS nanorod. The yellow arrow indicates scan direction (squared area was used for drift correction).

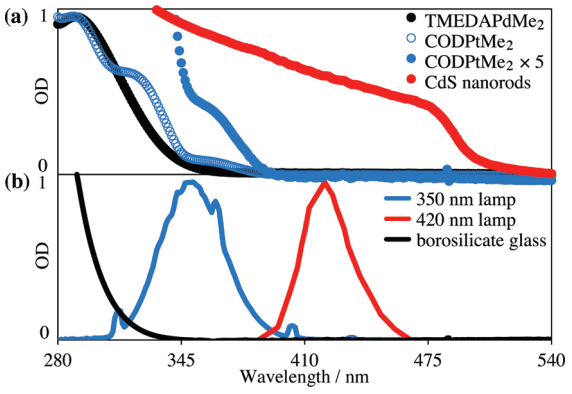

Figure 3. (a) Absorption spectra of $TMEDAPdMe_2$ (black), $CODPtMe_2$ (blue), and colloidal CdS rods (red) (recorded in toluene with quartz cuvettes). (b) Irradiance spectra of 350 nm (blue) and 420 nm (red) lamps and absorption spectrum of the borosilicate glass (black) used as reaction vessel (all spectra were arbitrarily normalized to a maximum optical density OD = 1).

(70%) are freestanding, unattached to CdS nanorods. Only a small fraction of Pt particles (30%) are bound to the surface of CdS nanorods (Table 1, entry 1) (Figure 1d). Among surface-bound particles, there is an average of 1.1 ± 0.9 Pt particles per CdS nanorod, with a maximum of three Pt particles per CdS nanorod (Figure 1e). The fact that freestanding Pt particles form thermally from the direct reaction between $CODPtMe_2$ and triethylamine indicates that Pt particles can form independently from CdS and that preformed Pt particles do not tend to associate with CdS nanorods after they have already formed.

We then carried out metal deposition experiments under photochemical conditions and observed different results depending on the specific lamp wavelength used. Photo deposition of Pt on CdS nanorods under illumination with a 350 nm lamp (35 nm fwhm) at room temperature results in the formation of Pt particles with a diameter of 2.6 ± 0.8 nm. A significant fraction of Pt particles (20%) formed under 350 nm illumination are still freestanding (remain unassociated with the CdS nanorods) (Table 1, entry 2). However, a larger fraction of Pt particles (80%) are bound to the surface of CdS nanorods (Figure 1d). Among surface-bound particles, there is an average of 1.6 ± 1.3 Pt particles per CdS nanorod, although we observed a few cases with as many as three, four, and six Pt particles per CdS nanorod (Figure 1e). Similarly, photo deposition of Pt on CdS nanorods under illumination with a 420 nm lamp (30 nm fwhm) at room temperature results in the formation of Pt particles with a diameter of 3.1 ± 1.4 nm (Figures 1 and 2). In this case, only a marginal number of Pt particles (5%) are freestanding (Table 1, entry 3). The greater majority of Pt particles (95%) formed under 420 nm illumination are bound to the surface of CdS nanorods (Figures 1d and 2). Among surface-bound particles, there is an average of 1.4 ± 0.9 Pt particles per CdS nanorod, with a maximum of three Pt particles per CdS nanorod (Figure 1e). In the absence of the CdS nanorods, the reaction between $CODPtMe_2$ and triethylamine under 350 nm illumination at room temperature results in the formation of Pt particles with a diameter of 2.9 ± 1.2 (Table 1, entry 4). The fact that Pt particles form by direct reaction between $CODPtMe_2$ and triethylamine under 350 nm illumination confirms that photochemical formation of freestanding Pt particles can occur independently from the CdS nanorods. CdS nanorods need not act as "sensitizers" for the decomposition of the organometallic precursor. Similar photochemical reactions have been reported for other metal particles and precursors.[49]

Site Selective Metal Photo Deposition: Free- versus Surface-Bound Metal Particles. The observations above are independent of the postsynthesis handling of samples, all of which were consistently worked up in the same way (see Experimental Section). Size selection was not performed. Instead, these observations suggest the existence of multiple parallel pathways for the formation of Pt nanoparticles. In order to better understand this, we recorded the absorption spectra of CdS nanorods

dx.doi.org/10.1021/cm201513a |*Chem. Mater.* 2011, 23, 3571–3579

Scheme 1. Metal Deposition Pathways

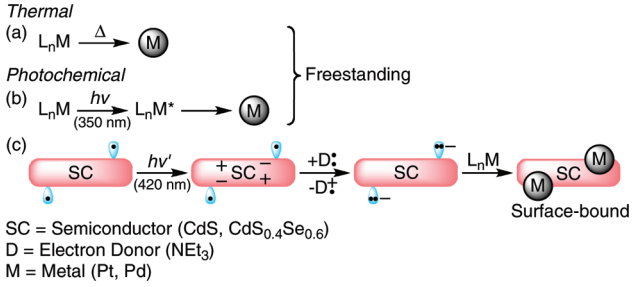

and the molecular Pt precursor, $CODPtMe_2$, in toluene solution (Figure 3a). CdS nanorods have an absorption band-edge at 500 nm and continue to absorb more strongly at shorter wavelengths. The $CODPtMe_2$ precursor is colorless and does not absorb in the visible region but has three distinct bands in the ultraviolet region: 285, 320, and 360 nm. Comparing these spectral features to the irradiance profiles of the two lamps used (Figure 3b), both CdS nanorods and $CODPtMe_2$ can absorb light emitted by the 350 nm lamp. In contrast, only CdS nanorods, not $CODPtMe_2$, can absorb light emitted by the 420 nm lamp.

Our experimental observations can be explained as follows: When the organometallic precursor $CODPtMe_2$ is heated in the dark, it decomposes thermally and nucleates into freestanding (unbound) Pt particles anywhere in solution (Scheme 1a). Under photochemical conditions, direct absorption by (and excitation of) the $CODPtMe_2$ in the presence of triethylamine results in photoinduced reduction and nucleation of freestanding (unbound) Pt particles anywhere in solution, as observed experimentally to some extent (15%)[48] with the 350 nm lamp (Scheme 1b).[48,50] Together, these thermal and photochemical homogeneous nucleation pathways are responsible for the formation of freestanding Pt nanoparticles independently of the semiconductor surface. Alternatively, under photochemical conditions, when absorption (and excitation) occurs through the CdS nanorods, a third pathway occurs where electron−hole pairs (excitons) are formed on the semiconductor followed by migration of electrons to surface trap states (dangling bonds)[8] on the semiconductor surface. Holes can be quenched by triethyl amine, sulfide ions, or other electron donor. The surface localized electrons can act as seeding points for the binding and reduction of $CODPtMe_2$ into Pt nuclei. This heterogeneous nucleation mechanism is responsible for the formation of bound Pt nanoparticles on the surface of CdS nanorods, as observed experimentally with both 350 and 420 nm lamps (Scheme 1c).

The observed site-selectivities (Table 1, entries 1−3) can be used to gather additional information about the metal photo deposition process. At 350 nm, the absorption coefficient of colloidal CdS nanoparticles is known to be of the order of $\varepsilon_{350\ nm} \approx 1.5 \pm 5 \times 10^6$ L mol^{-1} cm^{-1},[10] whereas we measured the absorption coefficient of $CODPtMe_2$ to be only $\varepsilon_{350\ nm} = 260 \pm 30$ L mol^{-1} cm^{-1}. Using these values to normalize the respective relative populations of surface-bound (80%) and freestanding (15%)[48] particles obtained photochemically with the 350 nm lamp, we calculate a 1000× (thousand-fold) *apparent preference* for photochemical Pt particle formation via homogeneous nucleation (in solution) over heterogeneous nucleation (on the CdS surface). This simple calculation assumes growth of Pt nanoparticles from Pt nuclei is fast and irreversible. It does not take into account energy barriers required for either homogeneous or heterogeneous nucleation. Also, it does not take into account the efficiency of charge collection by dangling bonds on the semiconductor surface (exciton quenching by trap states) or of platinum photoreduction by either mechanism (Scheme 1b,c). Additionally, this preference may vary depending on the chemical composition of the semiconductor surface (Cd- versus S-rich, ligand type and surface coverage, etc.).[2,8,49] We emphasize the above preference is just an *apparent* and yet-to-be-completed account of the relative ease of solution formation versus surface deposition of Pt particles under photochemical conditions.

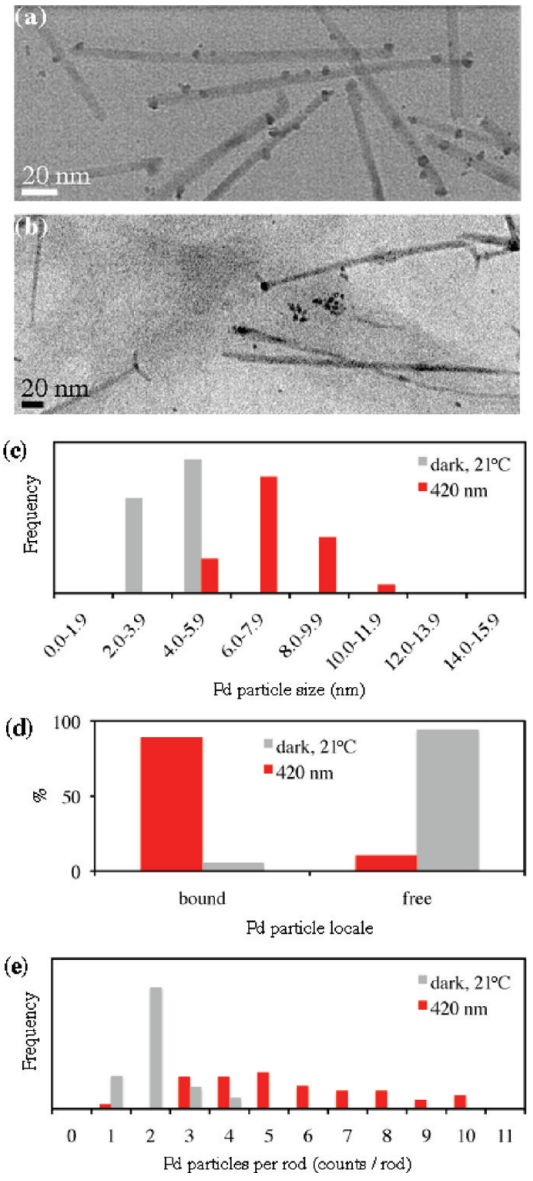

Figure 4. Sample TEM micrographs of CdS−Pd heterostructures prepared (a) photochemically (420 nm, 24 °C) and (b) thermally (in the dark, 24 °C). Pd particle size (c), locale (d), and loading per rod (e) histograms for CdS−Pd heterostructures prepared thermally (24 °C in the dark, gray) and photochemically (420 nm, red) (>50−100 CdS rods and >50−300 Pd particles measured in each case).

Palladium Deposition on CdS Nanorods. Using the optimized experimental conditions described above for Pt (illumination with a 420 nm lamp for 3 h at RT), we carried

dx.doi.org/10.1021/cm201513a |*Chem. Mater.* 2011, 23, 3571–3579

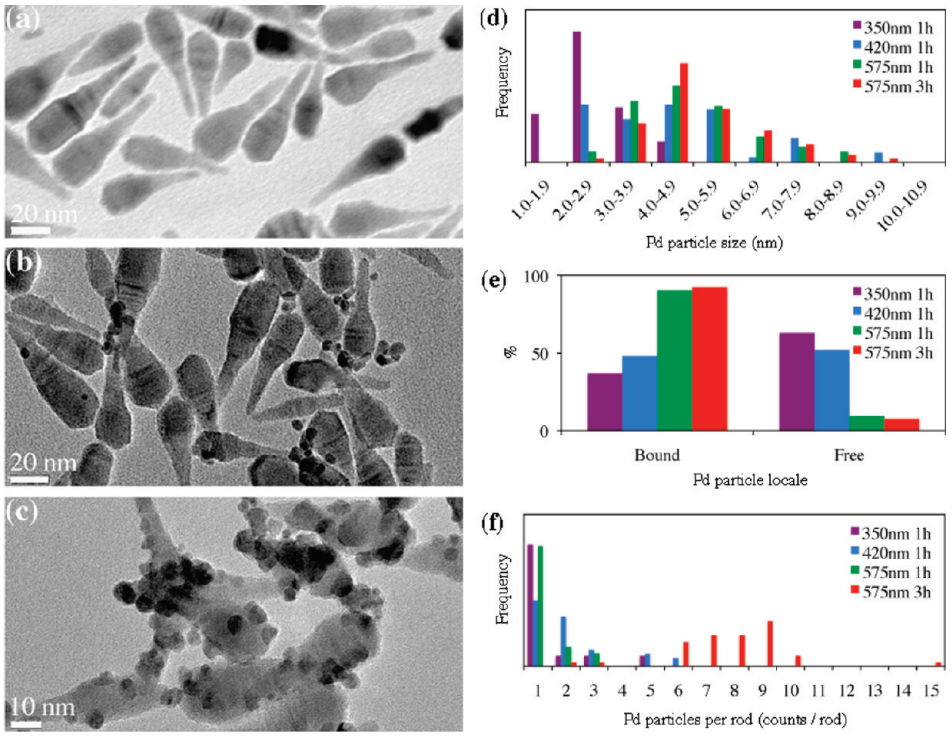

Figure 5. Sample TEM micrographs of $CdS_{0.4}Se_{0.6}$ nanorods (a), and $CdS_{0.4}Se_{0.6}$—Pd heterostructures prepared photochemically at 575 nm, 24 °C for 1 h (b) and 3 h (c). Pd particle size (d), locale (e), and loading per rod (f) histograms for $CdS_{0.4}Se_{0.6}$—Pd heterostructures prepared photochemically at 350 nm for 1 h (violet), 420 nm for 1 h (blue), 575 nm for 1 h (green), and 575 nm for 3 h (red) (>50—100 $CdS_{0.4}Se_{0.6}$ nanorods and >50—300 Pd particles measured in each case).

out the photo deposition of Pd on CdS nanorods using the molecular precursor cis-dimethyl(N, N, N′, N′-tetramethylenediamine)-palladium(II), $TMEDAPdMe_2$. In this case, Pd particles form with an average diameter of 7.2 ± 1.7 nm, the majority of which (90%) are bound to the CdS surface, and only a few (10%) are freestanding (Table 1, entry 5) (Figure 4a,c,d). Among surface-bound particles, there is an average of 5.6 ± 2.2 Pd particles per CdS nanorod and a maximum of 11 Pd particles per CdS nanorod (Figure 4e). Under these conditions, the Pd precursor appears to be more reactive and Pd deposition more facile, as judged by the larger Pd particle diameter and the higher number of Pd particles per rod compared to Pt. We attribute this difference to the inherent thermal and photochemical instability of $TMEDAPdMe_2$ compared to $CODPtMe_2$. Conversely, thermal deposition of Pd on CdS nanorods at room temperature in the complete absence of light results in the formation of Pd particles with a diameter of 4.1 ± 0.7 nm (Figure 4b,c). In agreement with our previous observations, the majority of the thermally deposited Pd particles (94%) are freestanding, and only a very few (6%) are bound to the surface of CdS nanorods (Table 1, entry 6) (Figure 4d). Among surface-bound particles, there is an average of 2.1 ± 0.7 Pd particles per CdS nanorod, with a maximum of four Pd particles per CdS nanorod (Figure 4e).

Palladium Deposition on Axially Anisotropic CdSSe Nanorods. We then attempted the photo deposition of Pd on axially anisotropic $CdS_{0.4}Se_{0.6}$ nanorods using $(TMEDA)PdMe_2$ as precursor. These $CdS_{0.4}Se_{0.6}$ nanorods have a graded-alloy composition between a thick CdSe-rich "head" on one end and a thin CdS-rich "tail" on the other end (Figures 5a and 6d).[46] Initial photo deposition experiments on these axially anisotropic nanostructures were directed at testing the degree of optoelectronic communication between small and large band gap segments; Pd particles can be deposited on both ends of the $CdS_{0.4}Se_{0.6}$ nanorods. However, we find illumination energy (lamp wavelength) and time both have a strong effect on the diameter, loading, and specific locale of the Pd particles obtained. Additionally, the distribution of Pd particles along the length of the axially anisotropic $CdS_{0.4}Se_{0.6}$ nanorods varies significantly depending on the specific lamp used.

Photo deposition of Pd on $CdS_{0.4}Se_{0.6}$ rods for 1 h at RT results in 2.6 ± 0.8 nm diameter Pd particles with an average of 1.5 ± 1.1 (5 max) Pd particles per rod when using a 350 nm lamp (35 nm fwhm), 4.9 ± 2.2 nm diameter Pd particles with an average of 2.1 ± 1.5 (6 max) Pd particles per rod when using a 420 nm lamp (30 nm fwhm), and 5.0 ± 1.5 nm diameter Pd particles with an average of 1.3 ± 0.8 (3 max) Pd particles per rod when using a 575 nm lamp (~75 nm fwhm) (Table 1, entries 7—9) (Figure 5). Further, photo deposition for 3 h at RT results in 5.1 ± 1.4 nm diameter Pd particles with an average of 8.0 ± 2.0 (15 max) Pd particles per rod when using a 575 nm lamp (Table 1, entry 10) (Figure 5). These results highlight interesting trends in metal particle size, loading, and locale during the metal photo deposition process. First, it appears that the Pd particle diameter may increase with increasing lamp wavelength for a given photo deposition time; however the standard deviations are too large to make the differences in Pd particle diameter statistically significant: 2.6 ± 0.8 nm (350 nm for 1 h), 4.9 ± 2.2 nm (420 nm for 1 h), and 5.0 ± 1.5 nm (575 nm for 1 h) (Table 1, entries 7—9) (Figure 5d). In contrast, the Pd particle diameter remains constant for different photo deposition times,

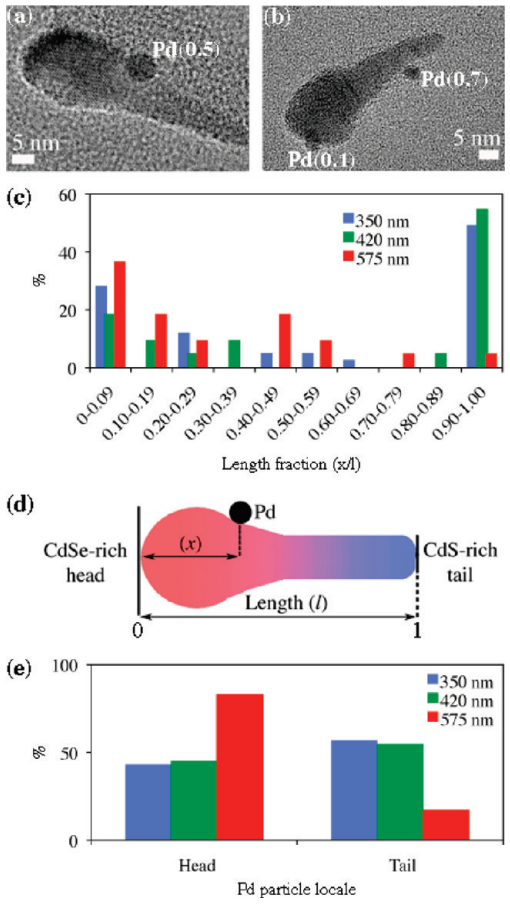

Figure 6. Photodeposition of Pd nanoparticles on axially anisotropic $CdS_{0.4}Se_{0.6}$ nanorods: (a) Sample TEM micrographs with Pd length fractions. (b) Location of Pd nanoparticles along the length of the $CdS_{0.4}Se_{0.6}$ nanorods, plotted as a fraction of the total length of the nanorods (length fraction). (c) Schematic of $CdS_{0.4}Se_{0.6}$–Pd heterostructures and length fraction measurements. (b) Head-side vs tail-side population of Pd nanoparticles on $CdS_{0.4}Se_{0.6}$ nanorods.

while keeping the wavelength constant: 5.0 ± 1.5 nm (575 nm for 1 h) ~ 5.1 ± 1.4 nm (575 nm for 3 h) (Table 1, entries 9–10) (Figure 5d).

In agreement with our previous observations, the fraction of surface-bound Pd particles increases with increasing lamp wavelength: 350 nm for 1 h (37% surface-bound) < 420 nm for 1 h (48% surface-bound) < 575 nm for 1 h (80% surface-bound) (Table 1, entries 7–9) (Figure 5e). Similary, the fraction of surface-bound Pd particles remains mostly unchanged with increasing photo deposition time for a given wavelength: 575 nm for 1 h (90% surface-bound) ~ 575 nm for 3 h (92% surface-bound) (Table 1, entries 9–10) (Figure 5e). This is consistent with our previous view that Pd and Pt particles form via semiconductor-mediated photochemical deposition and, unlike Au particles, freestanding Pd particles do not significantly stick to the surface of the $CdS_{0.4}Se_{0.6}$ nanorods after they formed. In turn, Pd loading (number of Pd particles per $CdS_{0.4}Se_{0.6}$ rod) remains approximately the same for different wavelengths, while keeping the photo deposition time constant: 1.5 ± 1.1 Pd particles/rod (350 nm for 1 h) ~ 2.1 ± 1.5 Pd particles/rod (420 nm for 1 h) ~ 1.3 ± 0.8 Pd particles/rod (575 nm for 1 h) (Table 1, entries 7–9) (Figure 5f). Nonetheless, Pd loading greatly increases with increasing photo deposition times while keeping the wavelength constant: 1.3 ± 0.8 Pd particles/rod (575 nm for 1 h) < 8.0 ± 2.0 Pd particles/rod (575 nm for 3 h) (Table 1, entries 9–10) (Figure 5f). This constitutes a 6-fold increase in Pd loading with tripling of the photo deposition time.

Site Selective Metal Photo Deposition: Head- versus Tail-Bound Metal Particles on Axially Anisotropic Nanorods. To better understand the locale and distribution of Pd particles on the axially anisotropic $CdS_{0.4}Se_{0.6}$ nanorods, we measured the distance between the axial position of each surface-bound Pd particle and one of the nanorod tips (arbitrarily chosen as the "head" tip) and then parametrized this distance by dividing it over the corresponding nanorod length (Figure 6a–d). In this way, the location of each surface-bound Pd particle is defined by a given "length fraction" that has a value between 0 (head tip) and 1 (tail tip) (Figure 6d). The advantage of using length fractions rather than absolute position values minimizes inhomogeneities associated with the distribution in nanorod lengths (59.3 ± 8.0 nm).[46] This way, the locale or position of many Pd particles can be better compared among several nanorods and across different photo deposition experiments. Using length fraction measurements, we discerned that photodeposited Pd particles preferentially accumulate toward one end or the other end of the axially anisotropic $CdS_{0.4}Se_{0.6}$ nanorods depending on the specific lamp wavelength used (Figure 6c). When we carry out the photo deposition using 350 and 420 nm lamps, a large fraction of the surface-bound Pd particles (≥50%) are located at or very near the tip of the thin CdS-rich tail of the $CdS_{0.4}Se_{0.6}$ nanorods with length fractions between 0.9 and 1 (Figure 6c). In contrast, when we carry out photo deposition with the 575 nm lamp, most of the surface-bound Pd particles (83%) are located on the thick CdSe-rich segment of the $CdS_{0.4}Se_{0.6}$ nanorods, with length fractions between 0 and 0.5 (Figure 6c). If instead of using length fractions, we divide each nanorod longitudinally in two half segments (at about 30 nm half length) and measure the fraction of Pd particles located on the thicker half segment versus those located on the thinner half segment, we observe similar trends in particle distribution. When we carry out the photo deposition using 350 and 420 nm lamps, 57% and 55%, respectively, of the surface-bound Pd particles are located on the thinner CdS-rich segment (Figure 6e). In contrast, when we carry out the photo deposition with the 575 nm lamp, 83% of the surface-bound Pd particles are located on the thicker CdSe-rich segment (Figure 6e).

These observations are relevant and somewhat resemble prior reports on metal (Au, Pd) photo deposition on CdSe/CdS seeded nanorods,where metal particles grow either close to the CdSe seed[16,29] or at the CdS-tips.[44] However, to the best of our knowledge, this manuscript is the first to document that metal photo deposition behavior can be controlled and utilized to achieve the site selective or "site-specific" photo deposition of metal particles on any specific segment of a heterostructure having an axial composition gradient. By switching the illumination energy to shorter or longer wavelengths while keeping all other experimental conditions constant (precursors, concentrations, temperature), the Pd particles can be controllably and site selectively photodeposited on either side of axially anisotropic $CdS_{0.4}Se_{0.6}$ nanorods (Figure 6c,e).

On the basis of the band edge position of pure CdSe (730 nm) and pure CdS (520 nm) phases (closer to 680 and 500 nm, respectively, as modeled by pure CdSe and pure CdS nanorods),[46] we can relate the differences in metal photo

dx.doi.org/10.1021/cm201513a |*Chem. Mater.* 2011, 23, 3571–3579

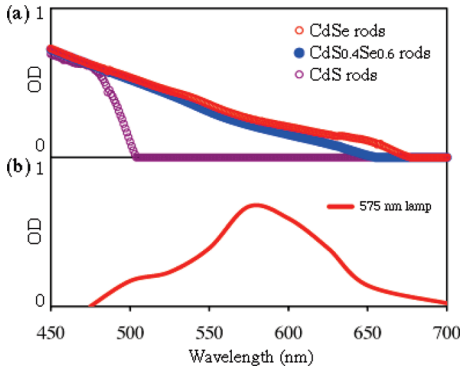

Figure 7. (a) Absorption spectra of colloidal CdS, $CdS_{0.4}Se_{0.6}$, and CdSe nanorods (recorded in toluene with quartz cuvettes), and (b) irradiance spectrum of 575 nm lamp (all spectra were arbitrarily normalized to a maximum optical density OD = 1).

deposition locale to the optical properties of the individual $CdS_{0.4}Se_{0.6}$ nanorod segments (Figure 7). The CdSe-rich head directly absorbs light emitted by all three 350, 420, and 575 nm lamps, allowing Pd particles to deposit on the head surface when the nanorods are irradiated with any of these wavelengths (Figure 7). In contrast, the CdS-rich tail only absorbs light emitted by the 350 and 420 nm lamps, but not light emitted by the 575 nm lamp, allowing Pd particles to deposit on the tail surface with the 350 and 420 nm lamps but not with the 575 nm lamp (Figure 7). The lower energy excitons produced with the 575 nm lamp appear to be localized on the head of the nanorods, and exciton trapping by surface defects must be rapid, given the strong effect the 575 nm lamp has in skewing the distribution of surface bound Pd particles toward the head of the nanorods. However, excitons appear able to travel relatively freely and uninterrupted across the whole length of the nanorods; we have observed Pd particles everywhere from the head tip to the tail tip of the nanorods with all the lamps, including the CdS-rich tail of the nanorods when using the 575 nm lamp (Figures 5c and 6a,b).

Among other factors that could affect metal deposition are the relative lamp intensities and relative nanorod absorption coefficients at each lamp wavelength. Lamp intensities determine the "power" or availability of photons and are independent of lamp wavelengths. Relative absorption coefficients determine how many photons are absorbed at each wavelength. Using 16 12-in. fluorescent lamps in each case, we measured the power (P) inside the Rayonette reactor as 136 W/m^2 ($P_{350\ nm}$), 16.6 W/m^2 ($P_{420\ nm}$), and 47.2 W/m^2 ($P_{575\ nm}$). Using the absorption spectrum of $CdS_{0.4}Se_{0.6}$ nanorods (Figure 7), we extract the following order of absorption coefficients: 5.4 ($\varepsilon_{350\ nm}$) > 3.5 ($\varepsilon_{420\ nm}$) > 1 ($\varepsilon_{575\ nm}$). Taking the products of lamp intensities and relative absorption coefficients, we obtain the following order: 16 ($P \cdot \varepsilon_{575\ nm}$) > 1.2 ($P \cdot \varepsilon_{420\ nm}$) $\approx$ 1 ($P \cdot \varepsilon_{350\ nm}$). Thus, light absorption and the efficiency of exciton generation with the 350 nm lamp may be higher than with the 420 or 575 nm lamps. However, we have conducted several photo deposition experiments and have not yet found a significant correlation between power and metal particle diameter or photo deposition locale/site selectivity. Further studies are under way to sort out the precise effect of irradiation power on metal photo deposition behavior.

Additionally, at individual particle level, relative absorption coefficients between different nanorod segments could play an important role. For example, both CdS-rich tail and CdSe-rich head segments absorb light emitted by 350 and 420 nm lamps with similar absorption coefficients.[10] This may be why the distribution of length fractions for Pd particles using the 350 and 420 nm lamps is relatively wide (Figure 6c). Finally, surface defects are likely to be important in determining the exact locale of metal deposition. The diameter of CdS-rich tail segments (5.6 $\pm$ 0.8 nm) is significantly thinner than the diameter of CdSe-rich segments (17.8 $\pm$ 2.4 nm). Thinner nanorods have larger surface-to-volume ratios as well as a sharper curvature and an increased surface energy.[8] Assuming that both segments are equally passivated, we can expect thin CdS-rich tail to contain a larger concentration of surface defects. This could explain why a larger fraction of Pd particles form on the CdS-rich segment when using 350 and 420 nm lamps and why many Pd particles form at the tip of the CdS-rich tail where curvature is the sharpest.

CONCLUSIONS

In summary, we have studied site selective and site-specific synthesis of colloidal semiconductor–metal hybrid heterostructures using whole-flask illumination/lamp photo deposition methods. We have shown precise lamp wavelength and its irradiance profile are critical in controlling whether metal photo deposition occurs in solution via homogeneous nucleation or on the surface of a colloidal semiconductor via heterogeneous nucleation, leading to freestanding or surface-bound metal nanoparticles, respectively. Using a number of control and metal deposition experiments, we identified three fundamental pathways leading to metal nanoparticle formation. Two of these pathways, thermal and direct photochemical precursor decomposition, lead to homogeneous nucleation of metal nuclei anywhere in solution and result in formation of unbound freestanding metal nanoparticles. A third pathway, semiconductor-mediated photochemical seeding and reduction of the metal precursor, leads to heterogeneous nucleation of metal nuclei at the semiconductor surface and results in formation of surface-bound metal nanoparticles. We have used these observations to selectively deposit Pt and Pd particles particles on the surface of CdS nanorods and axially anisotropic $CdS_{0.4}Se_{0.6}$ nanorods as model systems. Furthermore, we have shown specific lamp irradiance profile is critical in controlling specific locale (site-specificity) and overall distribution of Pd nanoparticles deposited on axially anisotropic $CdS_{0.4}Se_{0.6}$ nanorods. We expect the ability to reliably and controllably prepare semiconductor–metal hybrid heterostructures by judicious selection of reaction conditions, in this case by careful selection of lamp wavelength and irradiation times, will have major impact on engineering and tailoring these materials to target specific optical, electronic, magnetic, and catalytic properties. Reliable syntheses will increase availability of these hybrid nanomaterials for their fundamental study and application. We are presently studying the mechanism of metal deposition in more detail and specifically the effect irradiation power/intensity may have on diameter and locale of resulting metal nanoparticles. We are also exploring the activity of the resulting hybrid materials in solar-to-chemical conversion of renewable feedstocks as well as the deposition of other catalytically relevant and magnetically active metals on the surface of a variety of heterostructured nanoscale semiconductors.

■ ASSOCIATED CONTENT

Supporting Information. XRD, EDX, and additional TEM data. This information is available free of charge *via* the Internet at http://pubs.acs.org/.

■ AUTHOR INFORMATION

Corresponding Author
*vela@iastate.edu.

■ ACKNOWLEDGMENT

This research is supported by the U.S. Department of Energy, Office of Basic Energy Sciences, Division of Chemical Sciences, Geosciences, and Biosciences through the Ames Laboratory. The Ames Laboratory is operated for the U.S. Department of Energy by Iowa State University under Contract DE-AC02-07CH11358. We thank Iowa State University (ISU), the U.S. Department of Energy Ames Laboratory Royalty Account, and the Institute for Physical Research and Technology (IPRT) for laboratory startup funds (J.V.), ISU Chemistry Department for a Women in Chemistry Award (T.P.A.R.), Yaqiao Wu for helpful discussions, and Andreja Bakac, Aaron Sadow, John Verkade and Keith Woo for initial access to equipment.

■ REFERENCES

(1) Costi, R.; Saunders, A. E.; Banin, U. *Angew. Chem., Int. Ed.* **2010**, *49*, 4878–4897.
(2) Cozzoli, P. D.; Pellegrino, T.; Manna, L. *Chem. Soc. Rev.* **2006**, *35*, 1195–1208.
(3) Vaneski, A.; Susha, A. S.; Rodríguez-Fernández, J.; Berr, M.; Jäckel, F.; Feldmann, J.; Rogach, A. L. *Adv. Funct. Mater.* **2011**, *21*, 1547–1556.
(4) Kamat, P. V. *J. Phys. Chem. C* **2007**, *111*, 2834–2860.
(5) Shi, W.; Sahoo, Y.; Zeng, H.; Ding, Y.; Swihart, M. T.; Prasad, P. N. *Adv. Mater.* **2006**, *18*, 1889–1894.
(6) Franklin, A. D.; Smith, J. T.; Sands, T.; Fisher, T. S.; Choi, K.-S.; Janes, D. B. *J. Phys. Chem. C* **2007**, *111*, 13756–13762.
(7) Zhong, D. K.; Cornuz, M.; Sivula, K.; Grätzel, M.; Gamelin, D. R. *Energy Environ. Sci.* **2011**, *4*, 1759–1764.
(8) Smith, A. M.; Nie, S. *Acc. Chem. Res.* **2010**, *43*, 190–200.
(9) Talapin, D. V.; Lee, J.-S.; Kovalenko, M. V.; Shevchenko, E. V. *Chem. Rev.* **2010**, *110*, 389–458.
(10) Yu, W. W.; Qu, L.; Guo, W.; Peng, X. *Chem. Mater.* **2003**, *15*, 2854–2860. **2004**, *16*, 560–560.
(11) García-Santamaría, F.; Chen, Y. F.; Vela, J.; Schaller, R. D.; Hollingsworth, J. A.; Klimov, V. I. *Nano Lett.* **2009**, *9*, 3482–3488.
(12) Cademartiri, L.; Bertolotti, J.; Sapienza, R.; Wiersma, D. S.; von Freymann, G.; Ozin, G. A. *J. Phys. Chem. B* **2006**, *110*, 671–673.
(13) Nozik, A. J. *Chem. Phys. Lett.* **2008**, *457*, 3–11.
(14) Klimov, V. I. *J. Phys. Chem. B* **2006**, *110*, 16827–16845.
(15) Costi, R.; Saunders, A.; Elmalem, E.; Salant, A.; Banin, U. *Nano Lett.* **2008**, *8*, 637–641.
(16) Menagen, G.; Macdonald, J. E.; Shemesh, Y.; Popov, I.; Banin, U. *J. Am. Chem. Soc.* **2009**, *131*, 17406–17411.
(17) Carbone, L.; Jakab, A.; Khalavka, Y.; Sönnichsen, C. *Nano Lett.* **2009**, *9*, 3710–3714.
(18) Mokari, T.; Rothenburg, E.; Popov, I.; Costi, R.; Banin, U. *Science* **2004**, *304*, 1787–1790.
(19) Chakrabortty, S.; Yang, J. A.; Tan, Y. M.; Mishra, N.; Chan, Y. *Angew. Chem., Int. Ed.* **2010**, *49*, 2888–2892.
(20) Mokari, T.; Sztrum, C. G.; Salant, A.; Rabani., E.; Banin, U. *Nat. Mater.* **2005**, *4*, 855–863.
(21) Maynadié, J.; Salant, A.; Falqui, A.; Respaud, M.; Shaviv, E.; Banin, U.; Soulantica, K.; Chaudret, B. *Angew. Chem., Int. Ed.* **2009**, *48*, 1814–1817.
(22) Deka, S.; Falque, A.; Bertono, G.; Sangregoria, C.; Poneti, G.; Morello, G.; De Giorgi, M.; Giannini, C.; Cingolani, R.; Manna, L.; Cozzoli, P. D. *J. Am. Chem. Soc.* **2009**, *131*, 12817–12828.
(23) Habas, S. E.; Yang, P.; Mokari, T. *J. Am. Chem. Soc.* **2008**, *130*, 3294–3295.
(24) Shemesh, Y.; Macdonald, J. E.; Menagen, G.; Banin, U. *Angew. Chem., Int. Ed.* **2011**, *50*, 1185–1189.
(25) Pacholski, C.; Kornowski, A.; Weller, H. *Angew. Chem., Int. Ed.* **2004**, *543*, 4774–4777.
(26) Casavola, M.; Grillo, V.; Carlino, E.; Giannini, C.; Gozzo, F.; Pinel, E. F.; Garcia, M. A.; Manna, L.; Cingolani, R.; Cozzoli, P. D. *Nano Lett.* **2007**, *7*, 1386–1395.
(27) Saunders, A. E.; Popov, I.; Banin, U. *J. Phys. Chem. B* **2006**, *110*, 25421–25429.
(28) Elmalem, E.; Saunders, A. E.; Costi, R.; Salant, A.; Banin, U. *Adv. Mater.* **2008**, *20*, 4312–4317.
(29) Dukovic, G.; Merkle, M. G.; Nelson, J. H.; Hughes, S. M.; Alivisatos, A. P. *Adv. Mater.* **2008**, *20*, 4306–4311.
(30) He, S.; Zhang, H.; Delikanli, S.; Qin, Y.; Swihart, M. T.; Zeng, H. *J. Phys. Chem. C* **2009**, *113*, 87–90.
(31) Plante, I. J.; Habas, S. E.; Yuhas, B. D.; Gargus, D. J.; Mokari, T. *Chem. Mater.* **2009**, *21*, 3662–3667.
(32) Yang, J.; Elim, H. I.; Zhang, Q.; Lee, J. Y.; Ji, W. *Angew. Chem., Int. Ed.* **2011**, *50*, 1185–1189.
(33) Bao, N.; Shen, L.; Takata, T.; Domen, K. *Chem. Mater.* **2008**, *20*, 110–117.
(34) Bühler, N.; Meier, K.; Reber, J.-F. *J. Phys. Chem.* **1984**, *88*, 3261–3268.
(35) Reber, J.-F.; Rusek, M. *J. Phys. Chem.* **1986**, *90*, 824–834.
(36) Rufus, I. B.; Viswanathan, B.; Ramakrishnan, V.; Kuriacose, J. C. *J. Photochem. Photobiol. A* **1995**, *91*, 63–66.
(37) Uchihara, T.; Abe, H.; Matsumura, M.; Tsobumura, H. *Bull. Chem. Soc. Jpn.* **1989**, *62*, 1042–1046.
(38) Furlong, D. N.; Grieser, F.; Hayes, D.; Hayes, R.; Sasse, W.; Wells, D. *J. Phys. Chem.* **1986**, *90*, 2388–2396.
(39) Park, H.; Choi, W.; Hoffman, M. R. *J. Mater. Chem.* **2008**, *18*, 2379–2385.
(40) Jang, J. S.; Choi, S. H.; Kim, H. G.; Lee, J. S. *J. Phys. Chem. C* **2008**, *112*, 17200–17205.
(41) Ivanov, S. A.; Piryatinski, A.; Nanda, J.; Tretiak, S.; Zavadil, K. R.; Wallace, W. O.; Werder, D.; Klimov, V. I. *J. Am. Chem. Soc.* **2007**, *129*, 11708–11719.
(42) Gross, D.; Susha, A. S.; Klar, T. A.; Da Como, E.; Rogach, A. L.; Feldmann, J. *Nano Lett.* **2008**, *8*, 1482–1485.
(43) Menagen, G.; Mocatta, D.; Salant, A.; Popov, I.; Dorfs, D.; Banin, U. *Chem. Mater.* **2008**, *20*, 6900–6902.
(44) Li, X.; Lian, J.; Lin, M.; Chan, Y. *J. Am. Chem. Soc.* **2011**, *133*, 672–675.
(45) Robinson, R. D.; Sadtler, B.; Demchenko, D. O.; Erdonmez, C. K.; Wang, L.-W.; Alivisatos, P. *Science* **2007**, *317*, 355–358.
(46) Ruberu, T. P. A.; Vela, J. *ACS Nano* **2011**, *5*, in press.
(47) Chan, S. C.; Barteau, M. A. *Langmuir* **2005**, *21*, 5588–5595.
(48) Of the 20% unbound Pt particles observed, about 5% Pt particles are formed thermally at RT, as observed with the 420 nm lamp (Table 1, entries 2−3).
(49) Sakamoto, M.; Fujistuka, M.; Majima, T. *J. Photochem. Photobio. C: Photochem. Rev.* **2009**, *10*, 33–56.
(50) Luo, X.; Imae, T. *J. Mater. Chem.* **2007**, *17*, 567–571.